Heat and Mass Transfer Research Journal
Vol. 4, No. 1; 2020
Published by CanSRG
http://cansrg.com/journals/hmtrj/

Airfoil deposition and mist injection for enhancing film cooling effectiveness in gas turbine blades

Muhammad Awais, Saydus Salehin and Md. Hamidur Rahman*

Department of Mechanical and chemical Engineering, Islamic University of Technology (IUT), Board Bazar, Gazipur-1704, Dhaka, Bangladesh

Abstract

Gas turbines components such as vanes (nozzles), blades, and combustor liners are exposed to predominantly higher temperature while in operation. To sustain better performance of such components various critical conventional cooling techniques, e.g. air-film cooling, impingement jet cooling, inclusions of tabulators are employed. In this numerical study a novel technique has been employed with air/stream film cooling. The symmetric airfoil as deposition is used on 2D-flat plate surface to further improve the cooling performance of conventional air-film cooling techniques. Furthermore, water droplets are injected (mist injection) in cooling jet to concede the augmentation of local and average centerline film cooling effectiveness in downstream regions. This prediction of two-phase flow (continuous and discrete) is investigated by utilizing discrete phase model (DPM). The comprehensive investigation on variation of various ratios of density, mass flux, momentum flux and velocity and their influences on cooling effectiveness is also performed. Results demonstrated the significant enhancement of low temperature regions in downstream due to the inclusion of airfoil deposition and hence higher cooling effectiveness was achieved. Moreover, substantial increment in cooling effectiveness was achieved with a small amount of mist injection (2% mist) into the coolant jet. The evaporation of mist in downstream regions increased lower temperature regions and enhanced the cooling performance. Lastly, it was concluded that higher density ratio (DR=2.74) and moderate blowing ratio (BR=3.01) with the insertion of airfoil deposition and mist injection yield 13.6% higher average centerline film cooling effectiveness ($\overline{\boldsymbol{\eta}}$) than conventional film cooling technique without the presence of mist injection and airfoil deposition.

Keywords: *Gas turbine Film cooling; Numerical; Mist; Airfoil*

Nomenclature

h	heat transfer coefficient
T^w	local wall temperature
T^f	film temperature
T^∞	mainstream temperature
T^c	coolant jet temperature
ρ_i	density of coolant jet
ρ_∞	density of mainstream
V_i	velocity of coolant jet
V_∞	velocity of mainstream
$\overline{\boldsymbol{\eta}}$	average centerline film cooling effectiveness
η	local centerline film cooling effectiveness
d	water droplets diameter
$\Re_m$	Mainstream Reynold number
M/BR	Mass flux ratio/Blowing ratio

1. Introduction

Gas turbines (GT) are extensively used in land-based power generation and for aircraft propulsion. To avail substantial enhancement in GT engine performance the prominent increment in rotor inlet temperature (RIT) is adopted. The augmentation in RIT tends to yield conspicuous thermal

* Corresponding author
Submitted: February 1, 2020 Accepted: April 15, 2020

efficiency and power output for GT. First stage turbine stator vanes and rotor blades are predominantly exposed to hot gases coming from the exit of combustor. The excessive rise in GT inlet temperature results in higher heat transfer to the turbine blades. The exposure of blades to high temperature environment induces thermal stresses to greater extent within the blade material and hence leads toward the declination in GT life-span and efficiency. As the operating temperatures surpasses the permissible temperature, the requirement for innovative cooling techniques upsurges in order to optimize the turbine blade performance at the cost of excessive RIT. External and internal convection cooling techniques impart noteworthy impact on supplementing turbine blade performance by exterminating thermal stresses along the vicinity of suction and pressure surfaces. The former technique (film cooling) incorporates the injection of secondary fluid at discrete locations along the surfaces exposed to severely high temperature environment which tends to provide significant thermal protection by cooling both in the immediate region of injection and in the downstream region. The later heat transfer enhancement technique (jet impingement and pin-fin cooling) provides internal cooling of blades which is attained by allowing the coolant to pass through the various internal serpentine passages and eradicating thermal load from outside of the blades [1].

Geometric and fluid mechanical variables in film cooling technique impart momentous role in controlling heat transfer characteristics when the crossflow interaction between mainstream and coolant jet transpires at blades outer surface [2]. Geometric parameters encompass jet injection hole pattern, spacing, shape, and angle of attack while fluid mechanical variables are comprised of coolant to mainstream ratios mass flux (M), density ratio (D.R.), momentum flux (I), and velocity ratio (V.R). These ratios are demonstrated as follows.

$$\mathrm{M} = \frac{\rho_i V_i}{\rho_\infty V_\infty}, \quad \mathrm{DR} = \frac{\rho_i}{\rho_\infty}, \quad \mathrm{I} = \rho_i \frac{(V|i)^2}{\rho_\infty (V|\infty)^2}, \quad \mathrm{VR} = \frac{V_i}{V_\infty} \tag{1}$$

External cooling techniques yield direct reduction of heat load on the blade surface in contrast to internal cooling techniques. To determine the net heat load (q″) into the component both gas-side heat transfer coefficient (h_0) and wall temperature (T_w) are acknowledged first. Heat flux (q″) without film injection is given as

$$q'' = h_0 (T_\infty - T_w) \tag{2}$$

where T_∞ and T_w represent mainstream temperature and local wall temperature without film injection, respectively. With the inclusion of film injection q″ can be demonstrated as

$$q'' = h(T_f - T_w) \tag{3}$$

To demonstrate the impact of film cooling on reduction of blade surface temperature, a new parameter film effectiveness (η) is introduced.

$$\eta = \frac{Tw - T\infty}{Tc - T\infty} \tag{4}$$

From Eq. 4, the dependency of film cooling effectiveness on three potential temperature is evident.

For decades researchers have performed innumerable experimental and numerical studies to augment film effectiveness by incorporating novel and innovative techniques. Sinha et al. [2] elucidated the experimental study to acknowledge the effect of various fluid mechanical variables such as blowing ratio, density ratio, velocity ratio, and momentum flux ratio on laterally averaged film cooling effectiveness ($\acute{\eta}$) and centerline adiabatic film cooling effectiveness (ηc). For coolant injection into the mainstream a row of holes with 35^0 impact angle was considered. The mainstream velocity and temperature were kept constant while variation in coolant temperature

and velocity were made. Results depicted significant enhancement in η_c for higher values of density ratio and blowing ratio of coolant jet at constant momentum flux ratio. Furthermore, the increment in momentum flux ratio and reduction in density ratio provided lower ηc as lateral spread of cooling jet was quite insignificant in that regard. Anderson et al. reported the experimental study to illustrate the influence of wide range of Mach number of mainstream flow (0.03-0.15), blowing ratio (1-3) and Reynold number (5,500-15,500) on film cooling effectiveness while keeping the density ratio constant (DR=1.8). The impact of boundary layer characteristics on shaped cooling holes was focused. Results demonstrated the significance enhancement in adiabatic film effectiveness when Reynolds number was augmented from 5,400 to 15,000, however higher blowing ratio provided comparatively lower effectiveness due to coolant jet separation et al. [3] presented experimental and numerical studies and introduced a novel concept to attain dramatic film cooling performance. The embedment of cylindrical holes in sine wave shaped trench with different trench depth and wave peak were implemented. Results demonstrated that this peculiar geometric arrangement induces anti-counter rotating vortices which in results increases the coolant spread between the holes. Moreover, the increment in wave peak and trench depth depicted significantly higher influence on enhancement of film cooling effectiveness [4]. On two separate studies, Singh et al. [5, 6] have conducted 2D-numerical study to demonstrate the effect of coolant jet injection from single slot onto the flat plate and acknowledged the film cooling effectiveness at wide range of geometric and fluid mechanical variables such as six different injection angles (ranging from 150 to 900), three mass flux ratios (ranging from 1 to 3), density ratios (ranging from 1.1 to 5) and Reynold number (ranging from 8×104 to 8×105). It was concluded that higher blowing ratio tends to yield prominent increment in film effectiveness while considering the specified injection angle and density ratio. Additionally, lower injection angles (150 to 450) tends to have noticeable effect on film effectiveness as compared to higher injection angles (750 to 900) [5-6]. Jia et al. [7] reported 3D-numerical study to concede the influence of different geometries of film cooling holes and swirling effect of coolant jet on film cooling effectiveness. Three various types of film cooling holes were considered (cylindrical, clover shape and compound angle) with inclination angle of 30^0 and positive and negative swirling direction was attained in swirling chamber by adjusting two small jet holes inclined at certain jet angle to vertical direction. By keeping the density ratio constant (DR=1.5) and considering different range of mass flux ratio (0.5 to 1.5) results demonstrated striking enhancement in cooling effectiveness due to the inclusion of swirling effect of coolant jet for all geometric configuration of cooling holes. Moreover, it was perceived that effectiveness is sensitive for compound angle hole to both swirling strength and swirling direction while approximate heat transfer enhancement was found in case of cylindrical and clover shape holes [7]. The influence of reverse/forward coolant injection on mainstream flow was inspected for improved film cooling effectiveness. This study was performed both experimentally and numerically at different attack angles (300 to 600) of cylindrical cooling hole, five various blowing ratios (ranging from 0.25 to 3), constant density ratio (0.91) and Reynolds number (3.75×105). Results demonstrated promising enhancement in film cooling with backward injection of coolant into the mainstream as compared to forward coolant injection. Moreover, the variation in attack angle seemed to have insignificant impact on film cooling for reverse injection case. Al-Hemayri [8] presented 2D-numerical studies using RNG k-ε turbulence model to demonstrate the performance of film cooling using adiabatic film effectiveness for blowing ratio ranging from 0.5 to 2 and jet angles ranging from 300 to 900. The optimal value of mass flux ratio was found (BR=0.8) which provided comparatively higher cooling effectiveness than other blowing ratios at injection angle of 30^0[9-10].

In this present numerical study substantial focus has been given on further advancement of cooling effectiveness by the implementation of symmetric airfoil type deposition and prediction of mist cooling by employing of discrete phase model (DPM). Furthermore, this study provides crucial insights into the impact of wide range of fluid mechanical variables such as ratios of density, velocity, mass flux and momentum flux on centerline film cooling effectiveness. The optimal value of these ratios tends to have considerable benefits while attaining the higher cooling effectiveness which is the foremost concern of this study.

2. Scope of Present Study

As discussed previously GT engine performance is augmented by enhancing the rotor inlet temperature (RIT). This excessive increment tends to induce thermal loads into the blade material and consequently degrade the turbine blades lifespan. This 2D- numerical study presents a novel technique (film cooling with inclusion of airfoil deposition and employment of mist injection) and demonstrates the pursuit for finding out optimum fluid mechanical variables which could yield substantial enhancement in cooling effectiveness. This study will be exceedingly useful for designers to avail noteworthy reduction in weight and operating cost of the cooling system by implementing more feasible cooling configuration in aero engines. This study is segregated into four different cases such as Case1, Case2, Case3 and Case4 for absolute comprehension of desired goals. Case1 depicts the baseline computational domain without the inclusion of airfoil deposition and particles injection, Case2 represents the inclusion of airfoil deposition without mist injection, Case3 signifies the mist injection in computational domain without deposition and lastly Case4 demonstrates the presence of both deposition and mist injection. The influence of various fluid mechanical variables is presented for all these cases to determine the optimal ratios which yield desired greater average and local film cooling effectiveness.

3. Configurations of Computational Domain

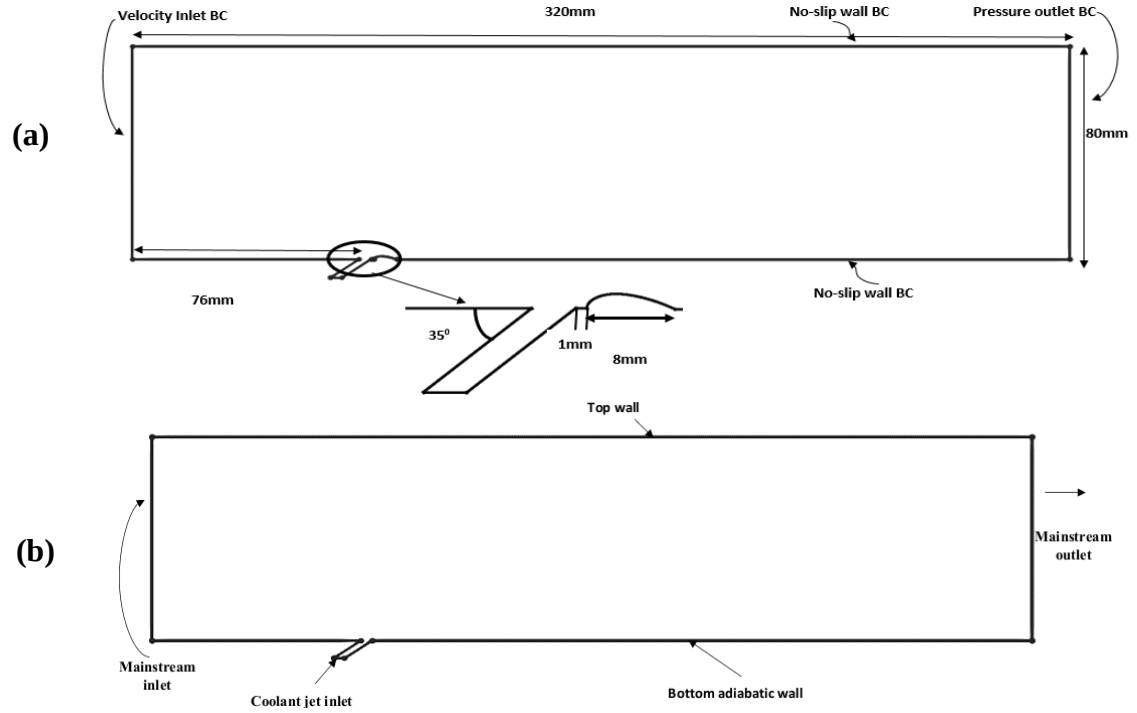

Figure 1. Computational domain (a) with airfoil deposition and (b) without deposition.

The computational domain in this study is 80D ×20D having slot width (D) of 4mm as demonstrated in Figure1a. The allocation of slot is 19d from the mainstream inlet while the vertical height of the jet hole is 1.74D. The inclination of coolant jet has noteworthy influence on availing the desired cooling effectiveness. On two separate studies, Singh et al. [5] and Bunker et al. [6] demonstrated the effect of various injection angles on film cooling effectiveness and recommended that lower injection angle tends to have significant influence on prevailing cooling effectiveness while preventing hot stream from permeating the blade surface [5,11]. Therefore, 350 injection angle is considered in this study to be optimal for obtaining better reduction in blade surface temperature [2]. A symmetric airfoil is used as deposition having constant span of 8mm located at a distance of 1mm from slot hole as depicted in Figure1b.

4. Numerical Approach

The commercial software ANSYS Fluent v12.0 has been used in this study. The simulation uses the segregated solver, which employs an implicit pressure correction scheme. To couple the pressure and velocity SIMPLEC algorithm was employed. To obtain des accuracy for spatial discretization of convective terms and species, second order upwind scheme was used. Discrete particle model (DPM) was adopted to investigate the interaction of dispersed phase with continuous phase, while DPM sources are updated every iteration. To model the discrete phase of water droplets the Lagrangian trajectory calculations were adopted, while the source terms of governing equations encompasses the impact of the droplets on the continuous phase. After attaining the flow field of continuous phase, the code traces the discrete phase trajectories, and computes the heat and mass transfer between the continuous phase and discrete phase.

4.1 Governing Equations

Governing equations such as incompressible continuity, momentum, energy and the equations for k-ε turbulence model are solved using ANSYS Fluent v12. Please refer to the Li et al.[13] for further details.

4.1.1 Discrete Phase (for water droplets)

Species transport Equation:

When coolant jet with water droplets enters mainstream, water droplet evaporates releasing water vapor into the mainstream, which requires consideration of species transport. In this study, three species are considered such as water vapor (H_2O), oxygen (O_2), and nitrogen (N_2). Species transport equation is given as

$$\frac{\partial}{\partial x_i}\left(\rho u_i C_j\right) = \frac{\partial}{\partial x_j}\left[\rho D_{eff,j}\frac{\partial C_j}{\partial x_i}\right] + \mathbf{S_j} \tag{5}$$

Here $\mathbf{C_j}$ denotes the mass fraction of one of the species (**j**) in the mixture while $\mathbf{S_j}$ represents source term for this species. Where $D_{eff,j}$ insinuate effective diffusion coefficient characterized by

$$D_{eff} = \mathrm{D} + \mu_t / Sc_t \tag{6}$$

Droplets velocity equation:

Various forces impart significant role in changing droplets velocity (v_p) in flow field such as hydrodynamic drag force (F_d), gravity force (F_g) and other forces (F_o) e.g. virtual mass force, thermophoretic force, Staffman's lift force, Brownian force etc. Eq. 7 depicts the relation for rate of change of droplet velocity due to external forces.

$$\frac{dv_p}{dt} = F_{g+} F_d + F_o \quad (7)$$

Mass change rate of droplets:

Since the mainstream temperature is comparatively higher than discrete phase (coolant jet/water droplet) which certainly leads toward the vaporization of water droplets in flow field. As rate of vaporization is characterized by the concentration difference between surface and mainstream then rate of mass change of droplets can be written as

$$\frac{dm_p}{dt} = \pi d^2 K_C (C_s - C_\infty) \quad (8)$$

where C_s and C_∞ signifies the vapor concentration at the droplet surface and vapor concentration of bulk flow, respectively. Transport equations are employed to avail the vapor concentration of bulk flow while C_s is assessed by considering the saturated flow over a surface. Furthermore, mass transfer coefficient (K_C) can be obtained by utilizing relation between Sherwood number (Sh) and Schmidt number (Sc).

$$Sh_d = \frac{K_c d}{D} = 2 + 0.6Sc^{0.33}Re^{0.5} \quad (9)$$

where D is the diffusion coefficient of the vapor in bulk flow.

Evaporation rate of water droplets:

The evaporation rate ($\frac{dm_p}{dt}$)can be determined using Eq. 20 when water droplet in bulk flow reaches to boiling point

$$\frac{dm_p}{dt} = \pi d^2 \left(\frac{\lambda}{d}\right) (2+0.46\Re_d{}^{0.5}) \ln (1+C_p(T_\infty - T)/h_{fg})/C_p \quad (10)$$

where $\Re_d, C_p \wedge \lambda$denotes Reynold number of water droplets, specific heat at constant pressure and thermal conductivity, respectively. The rate of sensible heat transfer between water droplets and hot stream demonstrates dependency on the convective heat transfer coefficient (h) and latent heat coefficient (h_{fg}) represented by

$$m_c c_p \frac{dT}{dt} = \pi d^2 h (T_\infty - T) + \frac{dm_p}{dt} h_{fg} \quad (11)$$

where convective heat transfer coefficient can be evaluated by an empirical correlation of Nusselt number (Nu) [12].

$$Nu = \frac{hd}{k} = 2 + 0.6Pr^{0.33}\Re_d{}^{0.5} \quad (12)$$

where $\Re_d$ is Reynold number for water droplets and Pr is Prandtl number.

Water droplet evaporation time:

Since water droplets characteristic velocity is considered to be in micrometer in this study which in results hold significantly lower Reynold number ($\Re_d$than bulk flow. In addition, the term $c_p(T_\infty - T)/h_{fg}$ is also significantly small (0.046) at DR=1.33. Hence Eq. 23 for droplet evaporation time can be obtained by arranging Eq 20 while substituting

$\Re_d$=1 and ln $(1+c_p(T_\infty - T)/h_{fg}) = c_p(T_\infty - T)/h_{fg}$.

i.e.

$$\boldsymbol{t} = \frac{h_{fg}\rho d^2}{2\lambda(T_\infty - T)} \quad (13)$$

Stochastic Particle Tracking

In stochastic particle tracking approach instantaneous fluid velocity ($u = \acute{u}+u'$) is used rather than average flow velocity $\acute{u}$ to predict the turbulent dispersion of particles/droplets by integrating the trajectory equations for individual particles. The velocity fluctuations are evaluated as

$$\mathbf{u}' = \zeta \left(u'^2\right)^{0.5} = \zeta \left(\frac{2k}{3}\right)^{0.5} \quad (14)$$

Here ζ signifies a normally distributed random number. The characteristic lifetime of eddy (t_e) is demonstrated either as a constant.

$$t_e = 2T_L \quad (15)$$

or as a random variation about T_L

$$t_e = -T_L \log(r) \quad (16)$$

where r is defined as a random variable between 0 and 1 and fluid Lagrangian integral time (T_L) is written as follows.

$$T_L = C_L \frac{k}{\varepsilon} \quad (17)$$

Here C_L is time scale constant.

$$T_L = 0.15 \frac{k}{\varepsilon} \quad (18)$$

By incorporating the Lagrangian integral time equations in characteristic lifetime of eddy equations, following expressions are obtained,

$$t_e = \frac{0.3k}{\varepsilon} \quad (19)$$

$$t_e = -0.15k/\varepsilon \log(r) \quad (20)$$

If the droplet slip velocity is much large i.e. time required for the droplet to cross the eddy is shorter than the time defined above, then the droplet eddy crossing time will be employed, which is indicated as

$$t_{cross} = -t_p \ln \left[\frac{1-Le}{t_p \vee u-u_p \vee}\right] \quad (21)$$

where L_e is the eddy length scale, $u - u_p \vee$ is magnitude of the relative velocity and t_p is the particle relaxation time defined as

$$t_p = \frac{\rho_p {d_p}^2}{18 \rho_g v_g} \quad (22)$$

To attain full trajectory of particles, instantaneous velocity is updated with a new normally distributed random number (**ζ**) after the particle relaxation time (t_p).

4.2 Boundary Conditions

To acquire desired validation without mist injection where the mainstream is considered to be dry air and coolant jet is saturated air, same flow velocity (10 m/s) for both mainstream and coolant jet is employed while mainstream and coolant temperatures were 400K and 300K respectively. However, to acknowledge the impact of various fluid mechanical variables on film cooling effectiveness flow velocity and temperature of coolant jet are varied for simulations with and without the mist injection while keeping the mainstream velocity and temperature constant (20m/s and 400K respectively). The main boundary conditions are presented in Table 1. Where Table 2 represents 26 different cases with various ratios of density, mass flux, velocity and momentum flux. Furthermore, velocity ratios are considered different for performing desired grid independence and test validation i.e. mainstream velocity (Vm) is taken as 10m/s for case6 to case11 while for other cases mainstream velocity is taken as 20 m/s. The variation in mainstream

velocity was adopted to examine the impact of two different Reynold numbers of mainstream (i.e. 30880 and 61760) on film cooling effectiveness. Similarly, coolant inlet temperature (Tc) was also kept different to acquire the influence of various DR on film cooling effectiveness while temperature for mainstream inlet is kept constant (T_m = 400k) for all the other cases as demonstrated in Table 2.

Table 1. Considered boundary conditions for simulations.

Zone	*Type*	*Applied boundary conditions*
Jet flow	*Velocity inlet*	*DPM: escape, V=Vc*
Mainstream	*Velocity inlet*	*DPM: escape, V=Vm*
Outlet	*Pressure outlet*	*0Pa, 300k*
Droplet Injection	--	*d=10μm, T=300k*
Top Wall	*No Slip*	--
Bottom Wall	*No Slip*	--
Side Wall	*Symmetry*	--

Table 2. Parameters considered in this study.

Case No	*Density ratio (DR)*	*Blowing Ratio (BR)*	*Coolant Jet Inlet velocity (V_c)*	*Mainstream inlet velocity (V_m)*	*Velocity ratio (VR)*	*Momentum flux ratio (I)*
1	1.14	1.029	18	20	0.9	0.926
2	1.14	2.00	35	20	1.75	3.5018
3	1.14	3.03	53	20	2.65	8.03
4	1.14	4.00	70	20	3.5	14.00
5	1.14	5.03	88	20	4.4	22
6	1.33	0.1333	1	10	0.1	0.0133
7	1.33	0.533	4	10	0.4	0.213
8	1.33	1.33	10	10	1	1.33
9	1.33	3.334	25	10	2.5	8.33
10	1.33	5.33	40	10	4	21.34
11	1.33	7.33	55	10	5.5	40.34
12	1.6	1.04	13	20	0.65	0.67
13	1.6	2.00	25	20	1.25	2.5
14	1.6	3.04	38	20	1.9	5.77
15	1.6	4	50	20	2.5	10
16	1.6	5.04	63	20	3.15	15.8
17	2.175	1.011	9.3	20	0.465	0.470
18	2.175	2.012	18.5	20	0.925	1.86
19	2.175	3.01	27.8	20	1.39	4.2
20	2.175	4.025	37	20	1.85	7.44
21	2.175	5.00	46	20	2.3	11.5
22	2.74	1.097	8	20	0.4	0.439
23	2.74	2.05	15	20	0.75	1.54
24	2.74	3.01	22	20	1.1	3.32
25	2.74	4.00	29.2	20	1.46	5.84
26	2.74	5.07	37	20	1.85	3.39

For mist cooling injection, uniform injection of water droplets in coolant jet from the slot inlet surface is implemented. Adequate selection of water droplet size and rate of mist injection needs

to be considered as their variation imparts substantial role in evaporation of mist into mainstream. Li et al.[13] demonstrated the impact of three different droplets size (5μm, 10μm and 15μm) and various mist rates (2% to 10%) on heat transfer coefficient and film cooling effectiveness through a 2D/3D numerical study. It was noticed that mist droplets with small size and rate at moderate Reynold number yield significant improvement in reduction of blade surface temperature. For example, at DR=1.33, d=10μm, and $T_\infty - T$ = 100K yield 0.032s evaporation time while at d=100μm evaporation time for water droplet reaches upto 324s. Therefore, in the present study 10μm droplet size and 2% mist rate were investigated at 3.5×10^5 droplet flow rate to concede their influence on film cooling effectiveness and further details can be found in [14].

4.3 Grid independence and convergence test

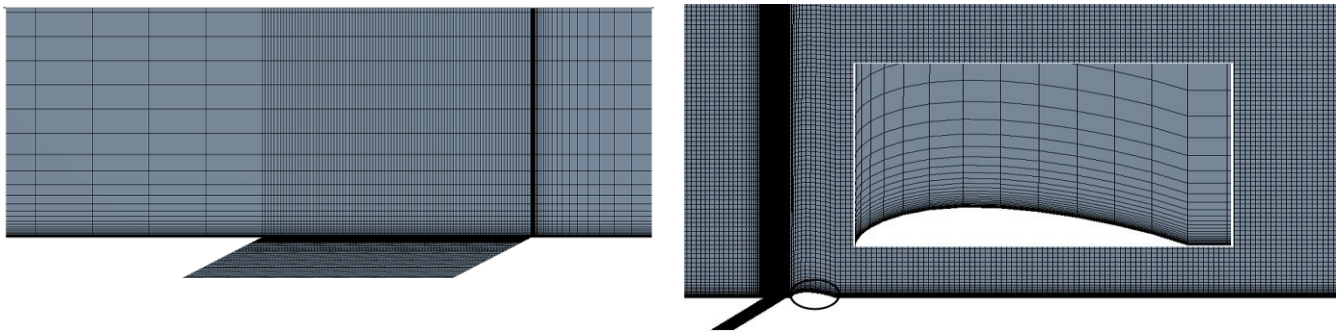

(a) **(b)**

Figure 2. Computational domain (a) with airfoil deposition and (b) without deposition.

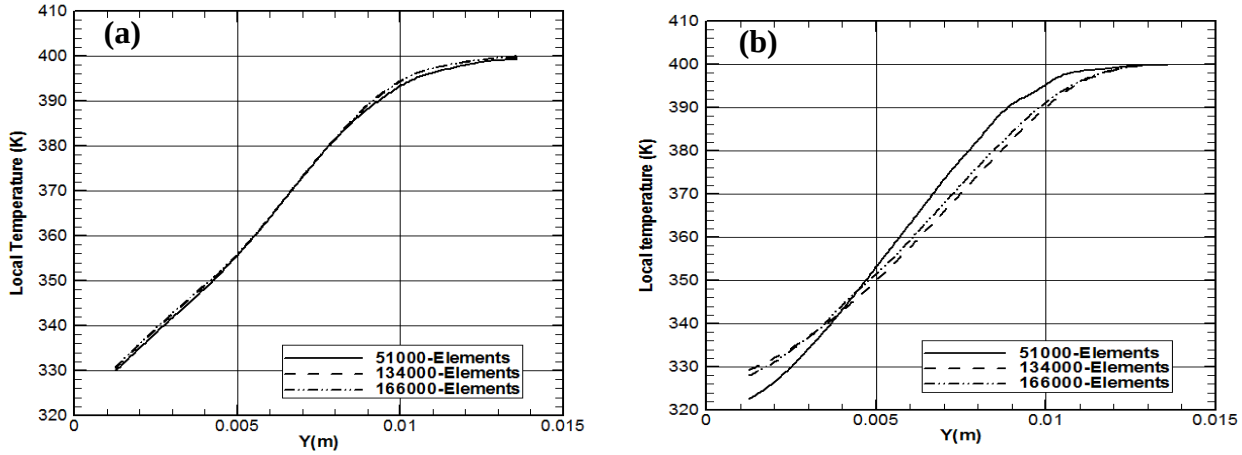

Figure 3. Grid independence study at X=0.1m, BR=1.33, DR=1.33 and $\Re_m$= 30880 for (a) Case1 and (b) Case2.

In numerical investigation three different uncertainties:1) Input uncertainty 2) Output uncertainty 3) Numerical uncertainty influence the numerical results. Numerical uncertainty occurs due to the guidance of discretization and iterative error. Therefore, prominent focus is given to mitigate the numerical uncertainty for acquiring desired outcomes. In this numerical study structured grids are adopted for 2D computational domain having denser regions near the jet slot, airfoil deposition and bottom wall as compared to top wall, mainstream inlet and mainstream outlet depicted in

Figure 2. For acquiring desired accuracy in results optimum values of Aspect ratio and Skewness were considered to keep the $\mathbf{y}^+$ value less than 1 near the bottom wall region. For grid independence test three different grid elements (51,000, 134,000 and 166,000) were considered for Case1 and Case2. Figure 3a and Figure 3b demonstrates the variation of temperature along the downstream region due to the different grid elements. For Case1 the effect of all three grid elements on temperature is insignificant, however for Case2 51,000 gird elements tends to have noticeable impact on temperature disparity. While the grid elements 134,000 and 166,000 show negligible influence on the heat transfer characteristics i.e. for Case2 at Y=0.0105m and X=0.1m local temperature deviation for 134,000 and 166,000 grid elements is 0.25%. Therefore, for rest of the simulations mesh with 134,000 grid elements were considered with considerable computational time and acceptable accuracy.

4.4 Enactment of Various Turbulence Models and Validation Test Study

For analyzing the effect of different turbulence models on cooling effectiveness, simulations were performed with five different models (k-ε standard wall treatment model, k-ε enhanced wall treatment model, k-ε-RNG enhanced wall treatment model, k-ω standard model and k-ω SST model) and comparisons were made with numerical study performed by Li et al. [14] without the mist injection and airfoil deposition as scrutinized in Figure4. It is quite evident that k-ε turbulence model with enhanced wall treatment yield comparatively lesser deviation in numerical results than other models due to its robustness for film cooling simulations. Furthermore, the influence of coolant injection on reduction of surface temperature along downstream region is quite significant i.e. the inclusion of coolant jet imparts substantial role in obtaining higher cooling effectiveness.

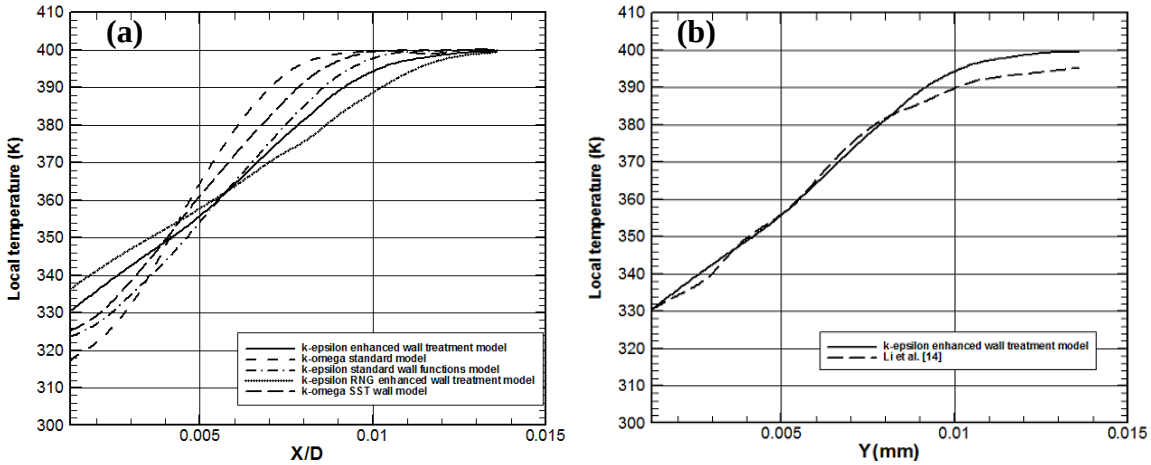

Figure 4. Validation study at BR=1.33, DR=1.33 and $\Re_m$= 30880 for Case1.

5. Results and Discussion

5.1 Film cooling effectiveness with airfoil deposition:

In this section the effect of various fluid mechanical variables, airfoil deposition and mist injection on average and local centerline film cooling effectiveness is extensively elucidated. The impact of variation+*- in ratios of density, velocity, mass flux and momentum flux on film cooling effectiveness is demonstrated through the depiction of graphs and contours while keeping the mainstream velocity constant.

5.1.1 Impact of Different Blowing ratios:

Blowing ratio is defined as the mass flux ratio of coolant jet to mainstream. The optimal value of blowing ratio yields noteworthy reduction in weight and operating cost of the cooling system which tends to make its implementation more feasible in aero engine cooling configuration. The augmentation in blowing ratio is obtained by increasing the coolant velocity/density or decreasing the mainstream velocity/density. In Figure 5a and Figure 5b the influence of different blowing ratios on average centerline film cooling effectiveness is depicted for both Case1 and Case2 respectively at constant mainstream velocity (20m/s) and different density ratios. It is quite evident that the collapse of $\acute{\eta}$occurs at lower blowing ratio which insinuates the attachment of coolant jet on the surface. However, at higher blowing ratio branch-offs appears between different data set of density ratios. In other words, it is fairly obvious that effectiveness tends to decrease at higher blowing ratio while optimal blowing ratio yield noticeably higher effectiveness for both cases [2]. This could be explained by a phenomenon that mainstream with higher flow velocity effortlessly dominates the coolant jet having lower flow velocity and its penetration into coolant jet stream increases. However, when coolant flow velocity increases the penetration effect reduces which in results surface temperature decreases and hence film effectiveness increases. However, excessive enhancement in blowing ratio jeopardizes the film cooling effectiveness. As significantly higher flow velocity of secondary flow provides poor protection to the surface exposed to higher temperature e.g. at DR=2.74 for Case1, at BR=2, BR=3 and BR=5 the average film effectiveness was found 0.74, 0.76 and 0.73 respectively. While at DR=2.74 for surface Case2, at BR=2, BR=3 and BR=5 the $\acute{\eta}$ was found 0.78, 0.79 and 0.75 respectively.

In Figure 5c and Figure 5d similar results are manifested which demonstrates the influence of various blowing ratio on local centerline film cooling effectiveness. It is quite evident that η is higher at the injection region of coolant for higher blowing ratios. However, this improved effect starts diminishing along the downstream regions and effectiveness reduces. This reduction is significantly lower for lower blowing ratio while comparatively higher for higher blowing ratio e.g. at DR=1.33 and X/D=10mm for Case1, at BR=0.533 and BR=3.33 the η is 0.67 and 0.97 respectively.

5.1.2 Influence of different density ratios:

The ratio of coolant jet density to mainstream density also imparts substantial role in availing the optimal film cooling effectiveness. As both blowing and density ratios are intertwined and demonstrates noticeable dependency on each other. In real GT engines, density of coolant is two times the density of mainstream. As coolant jet with lower temperature possesses different density than the mainstream with higher temperature. This density difference causes substantial influence on flow field and film cooling effectiveness. As to augment density ratio both mainstream and coolant jet velocities demands variation while keeping the mainstream Reynold number (Re_m) constant. In Figure5 it is quite evident that regardless of different blowing ratio values lower density ratio tends to yield lower average centerline film cooling effectiveness. However, as the density ratio rises average cooling effectiveness increases too e.g. at BR=3 for Case1, at DR=1.14 and DR=2.74 the $\acute{\eta}$ is 0.723 and 0.76 respectively. While for surface Case2 is 0.72 and 0.79 respectively. It is conspicuous that with the implementation of optimal blowing ratio (BR=3) and higher density ratio (DR=2.74) and with the inclusion of airfoil deposition the dramatic augmentation in centerline film cooling effectiveness can be achieved.

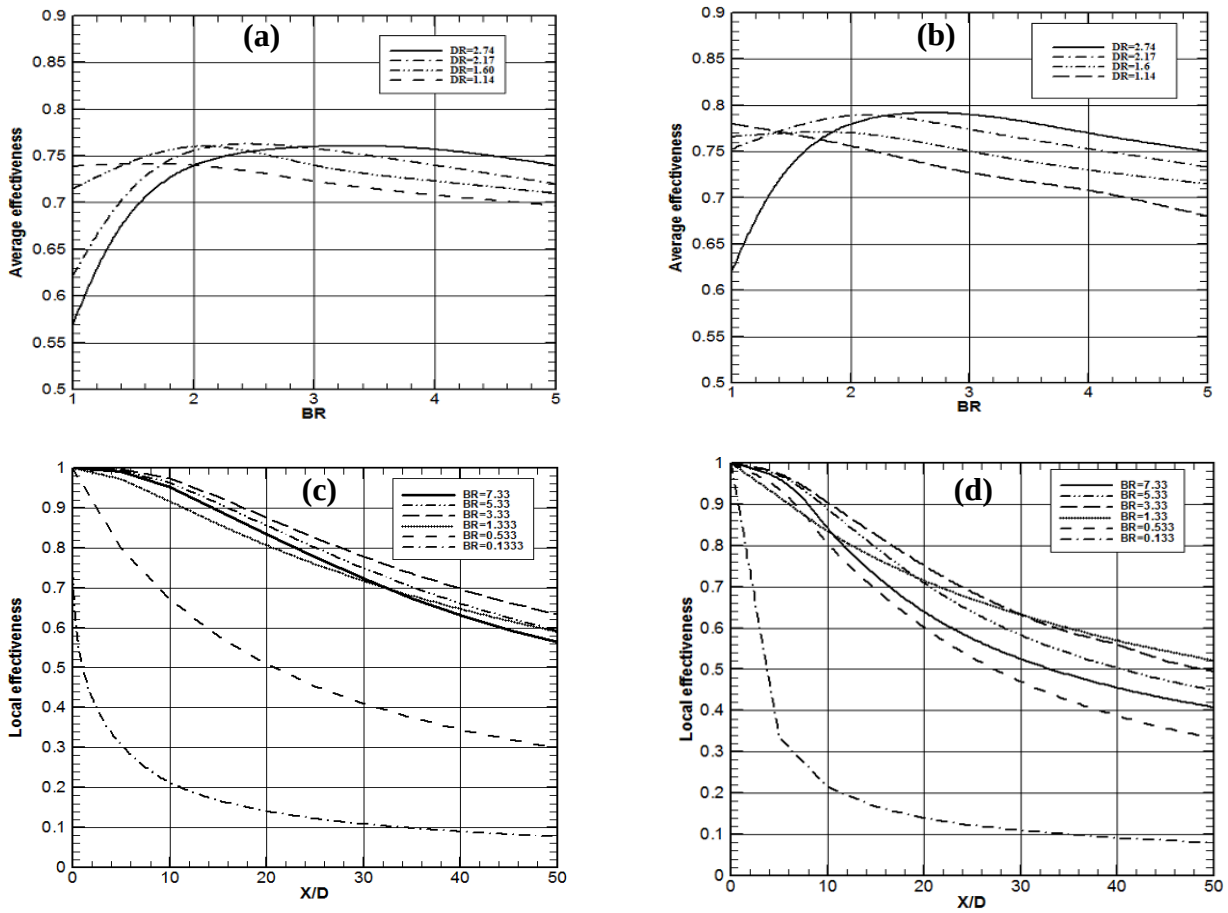

Figure 5. Influence of Blowing ratio on average centerline film cooling effectiveness at $\mathfrak{R}_m$=61760 for (a) Case1 (b) Case2 and Influence of Blowing ratio on local centerline film cooling effectiveness at $\mathfrak{R}_m$=61760 for (c) Case1 (d) Case2.

5.1.3 Influence of different velocity ratios:

For constant mainstream velocity and Reynold number, velocity ratio tends to decreases with the increment in density ratio. To avail economically feasible turbine engines incorporated with cooling configuration ratios of mass flux and velocity needs to have optimal values. In Figure 6a and Figure 6b the impact of various velocity ratios on $\overline{\boldsymbol{\eta}}$ is demonstrated for Case1 and Case2 respectively. It is evident that at lower density ratio $\bar{\eta}$ is substantially degraded at all values of VR, however, at higher DR prominent enhancement in $\bar{\eta}$ is achieved at quite lower VR. Furthermore, this effect is quite dominating when deposition is incorporated. The excessive enhancement in velocity ratio (VR) degrades the average cooling effectiveness $\overline{\boldsymbol{\eta}}$ regardless of various density ratio values. It can be explicated as for the fixed mainstream velocity (20m/s in this study) and different density ratios, various velocity ratios are obtained by increasing the coolant jet flow velocity as coolant velocity moderately higher than mainstream velocity protect the surface exposed to hot temperature even at far downstream regions resulting in augmented $\overline{\boldsymbol{\eta}}$.

5.1.4 Effect of different momentum flux ratio:

The momentum flux ratio (I) depicts significant reliance on mainstream flow velocity and coolant jet velocity as demonstrated in Eq. 1. The reduction of mainstream velocity/increment in coolant jet velocity provides higher mass flux ratio. Therefore, the variation of cooling effectiveness with

different ratios of velocity and mass flux appears quite the same i.e. for higher density ratios, the increment in momentum flux ratio yield greater average cooling effectiveness as compared to low density ratios presented in Figure 6c and Figure 6d for Case1 and Case2, respectively. However, at DR=2.74 and momentum flux ratio less than 2 tends to have comparatively lower effectiveness as low momentum flux ratio/velocity ratio signifies lower coolant jet velocity compared to mainstream velocity. This velocity reduction in coolant jet tends to minimize the lower temperature regions in downstream regions. In contrary, the higher ratios of mass flux and velocity insinuates excessive increment in coolant jet velocity than mainstream velocity. This significant enhancement in coolant jet velocity disturbs the mainstream flow and provide poor cooling film protection over the bottom surface exposed to hot mainstream.

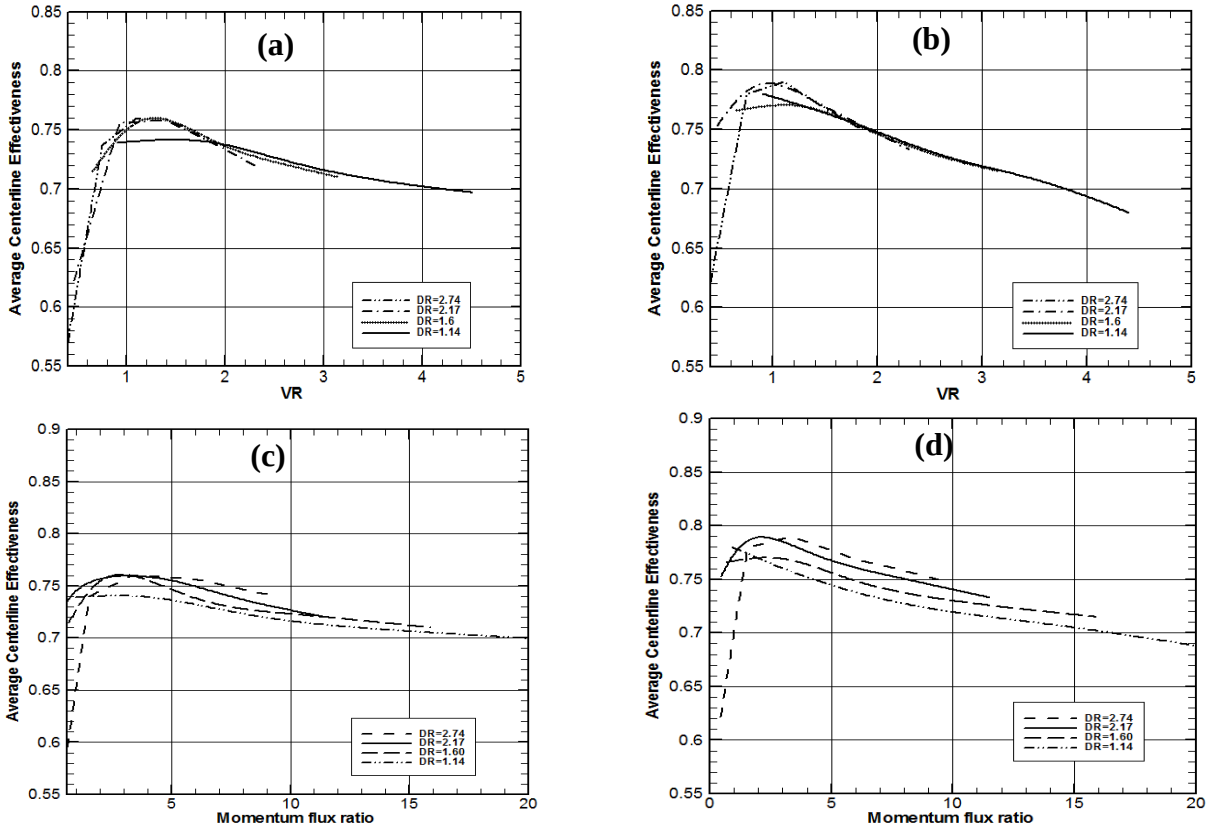

Figure 6. Impact of Velocity ratio on average centerline film cooling effectiveness at $\Re_m$=61760 (a) Case1 (b) Case2 and Impact of momentum flux ratio on average centerline film cooling effectiveness at $\Re_m$= 61760 (c) Case1 (d) Case2.

5.2 Film Cooling Effectiveness with Mist Injection

Mist injection impart noteworthy role in enhancing film cooling effectiveness. The water droplets are injected from coolant channel into the mainstream flow. Before interacting with cross flow, the water droplets tend to remain as liquid in coolant channel having no impact on variation of coolant jet velocity. As water droplets leaves the coolant channel and interacts with the mainstream flow, the evaporation starts and liquid phase of water droplets changes into vapor phase in mainstream flow. The vaporization of liquid droplets leads toward the expansion of volume flow rate which in results increases the flow rate of cooling stream yielding less requirement of cool air

bleeding from compressor. However, various crucial factors are considered which impart noticeable role in the vaporization of droplets into the mainstream flow e.g. droplets diameter, flow velocity of coolant jet and mainstream, mass flow rate of droplets etc. The effect of various ratios on film cooling effectiveness with mist injection is briefly discussed in this section.

5.2.1 Influence of various fluid mechanical variables:

The implementation of airfoil deposition yields wide range of low temperature regions predominantly in the downstream region. However, the supplementary extension of low temperature regions can be attained by the inclusion of mist injection with deposition which in results provide substantial augmentation in cooling effectiveness. Figure 7a demonstrates the impact of various density ratio, mass flux ratio and mist injection on average film cooling effectiveness of 2D-flat plate without deposition. The effect of increasing blowing ratio with different density ratio on cooling effectiveness is quite effective in the presence of water droplets. It is noticeable that enhancement in average film cooling effectiveness with the increment of both blowing ratio and density ratio in the presence of mist injection is noticeably higher e.g. at DR=2.74 and BR=2, for Case3 average cooling effectiveness $\overline{\eta}$ is 15.80% greater than the average cooling effectiveness for Case1. Moreover, Figure 7b portrays the striking enhancement in cooling effectiveness in the presence of both mist injection and airfoil deposition e.g. it was noticed that at DR=2.74 and BR=2 for Case4 $\overline{\eta}$ is 11.3% higher than Case2.

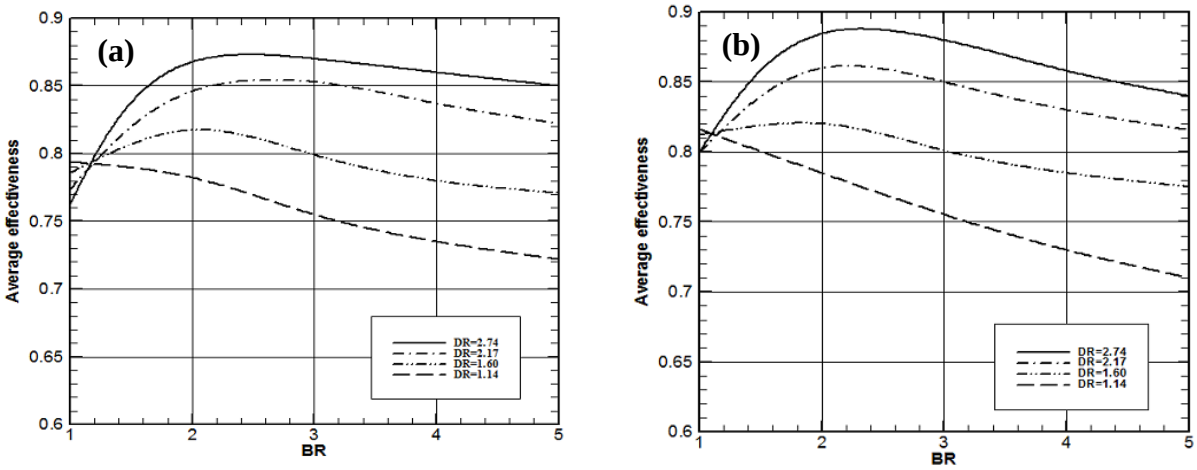

Figure 7. Impact of blowing ratio on average centerline film cooling effectiveness at M=2.0, DR=2.74, and Rem=61760 (a) Case3 (b) Case4.

Furthermore, the comparison in regards to the impact of film cooling between different cases is also demonstrated in Figure 8. It is quite clear that Case4 yields comparatively higher film cooling effectiveness than the other cases as the significant blanket-effect of the coolant layer with the mist injection comes into play yielding less interaction of mainstream with coolant jet at significant level. Moreover, the inclusion of adequately allocated symmetric airfoil deposition furtherly allows coolant jet to provide enhanced protection. However, cooling effectiveness performance at the far end of downstream regions for Case 3 and Case 4 seems quite the same.

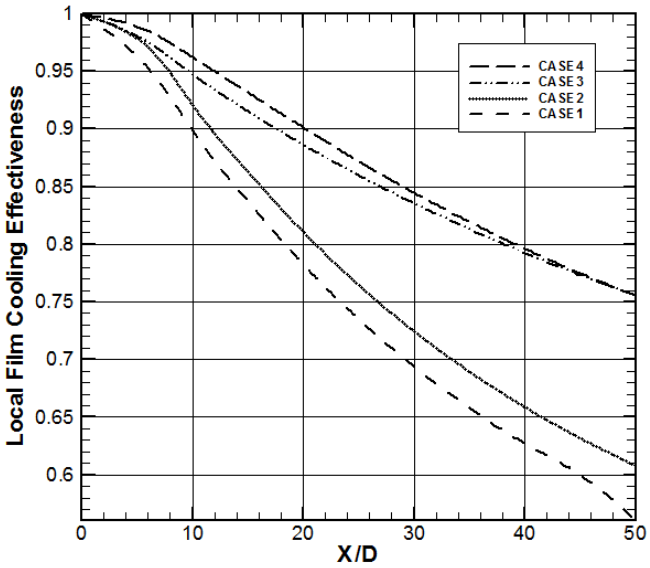

Figure 8. (a) For M=3.01, DR=2.74, and $\Re_m$=61760 Depiction of local centerline cooling effectiveness variation with different Cases.

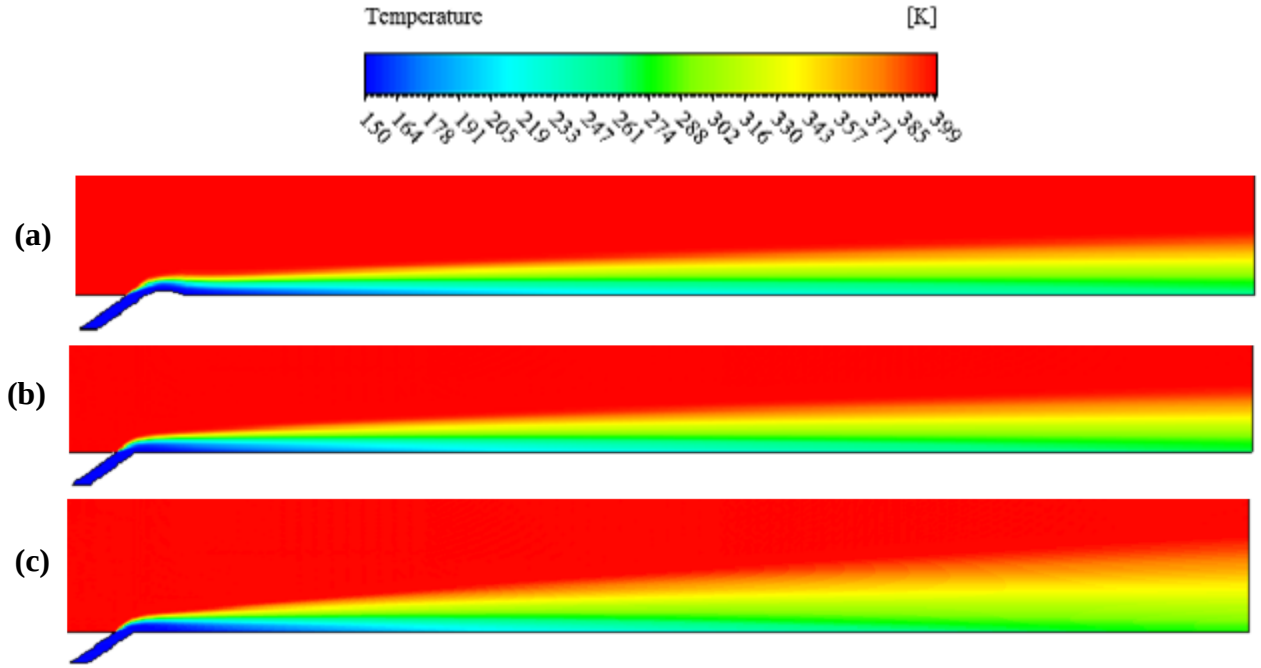

Figure 9: Temperature distribution at DR=2.74, BR=3.01R_m=61760 for (a) Case1 (b) Case2 and Temperature distribution at DR=2.74, BR=5 and R_m=61760 (c) Case1.

5.2.2 Flow Field Characteristics:

To visualize the impact of various fluid mechanical variables and geometric configuration of airfoil on flow field behavior, local and average centerline film cooling effectiveness temperature distributions and velocity contours are presented in this section. As conferred in previous sections, alternation in ratios of blowing, velocity, density and momentum flux induces prominent variations in heat transfer outcomes. Furthermore, the implementation of deposition and droplets injection also impart noteworthy influence on augmenting film cooling effectiveness.

Temperature distribution:

The enhanced protection for flat plate surface exposed to significantly higher mainstream temperature is attained by providing coolant film with the injection of coolant jet. Temperature contours are presented Figure 10a and Figure10b to visualize the effect of coolant jet at BR=3.01, DR=2.74 and $\Re_m$=61760 for Case1 and Case2. It is quite evident that airfoil deposition yields significantly greater local and average centerline film cooling effectiveness by providing lower temperature region which is extended far in the downstream region without instigating any disturbance in mainstream and preventing the excessive penetration of mainstream into coolant jet. Moreover, mass flux ratio higher than 3.01 tends to yield lower cooling effectiveness as its interaction with mainstream rises hence low temperature regions on bottom surface disappears as demonstrated in Figure 10c for Case1 at BR=5.00, DR=2.74 and $\Re_m$=61760. The substantial rise in η and $\overline{\eta}$ is availed by small amount of mist injection into coolant jet as lower temperature regions on bottom surface are further extended and provides ample prevention of mainstream penetration into coolant jet as depicted in Figure 11a and Figure 11b for Case3 and Case4 respectively at BR=3.01, DR=2.74 and $\Re_m$=61760. Moreover, with the inclusion of both airfoil deposition and mist injection greater effectiveness is achieved. As with the deposition first the coolant jet impinges on the airfoil deposition and then it flows over a bottom wall when the pressurized mainstream flow pushes it downwards in downstream region. Hence, the coolant jet flow with mist injection and airfoil deposition covers a large cooling area and yield significant reduction in temperature and prominent enhancement in cooling effectiveness.

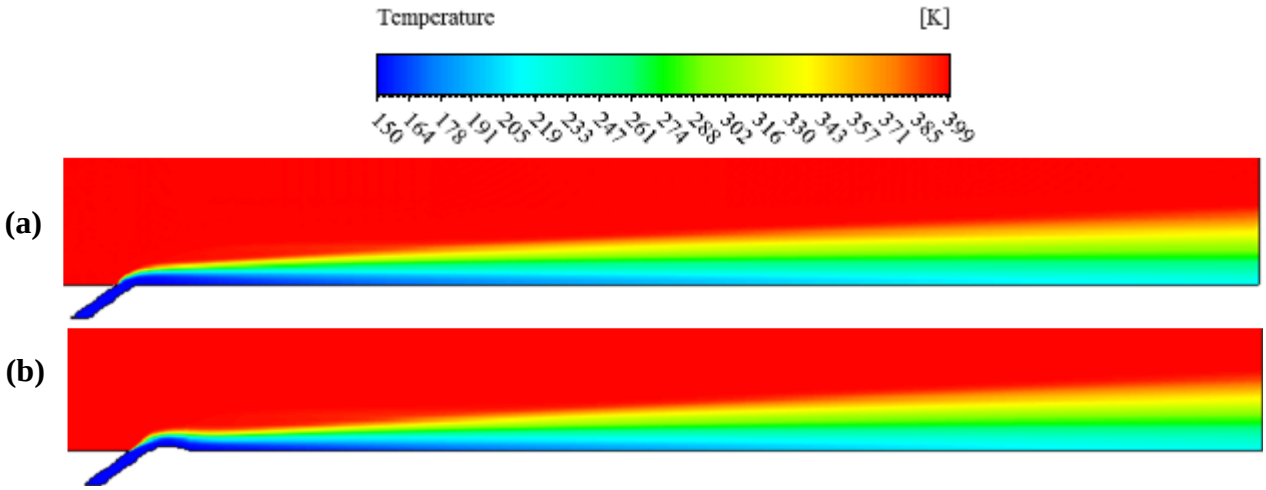

Figure 10. Temperature contour at DR=2.74, BR=3.01 and $\Re_m$=61760 (a) Case3 (b) Case4.

Velocity contours:

The effect of airfoil deposition on mainstream flow and coolant jet flow behavior is shown in Figure 12a and Figure 12b for Case1 and Case2 respectively at BR=3.01, DR=2.74 and $\Re_m$=61760. Mainstream flow velocity at the top wall surface is almost negligible due to no-slip boundary condition. However, the interaction of mainstream and coolant jet flow velocity is quite different for both cases on bottom wall surface. As airfoil directs the coolant jet flow in the mainstream region with the higher flow velocity due to its aerodynamic shape. Hence, at same blowing ratio (same mainstream and coolant jet velocity for both cases) for Case2 coolant jet flow covers a large area on bottom wall in downstream region as compared to

Case1 i.e. at BR=3, in the presence of deposition coolant jet flow possess enough capacity to prevent mainstream from disrupting the coolant flow behavior which impart striking role in obtaining the desired cooling effectiveness at optimum mass flux ratio.

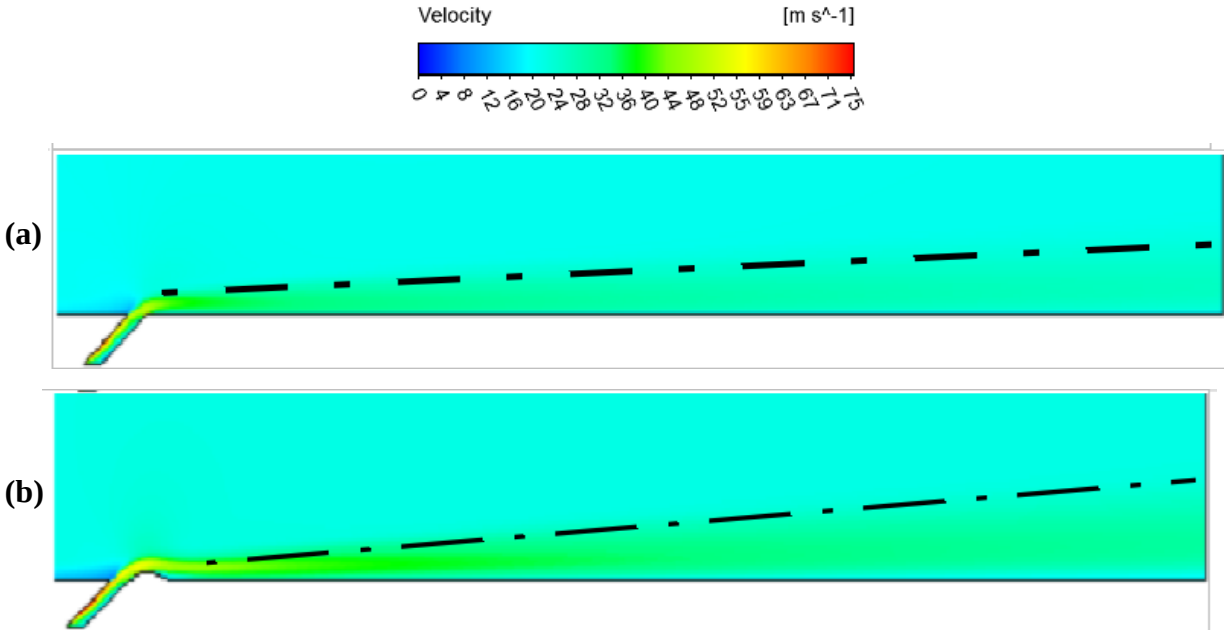

Figure 11. Velocity Contour at DR=2.74, BR=3.01, and R_m=61760 (a) Case1 (b) Case2.

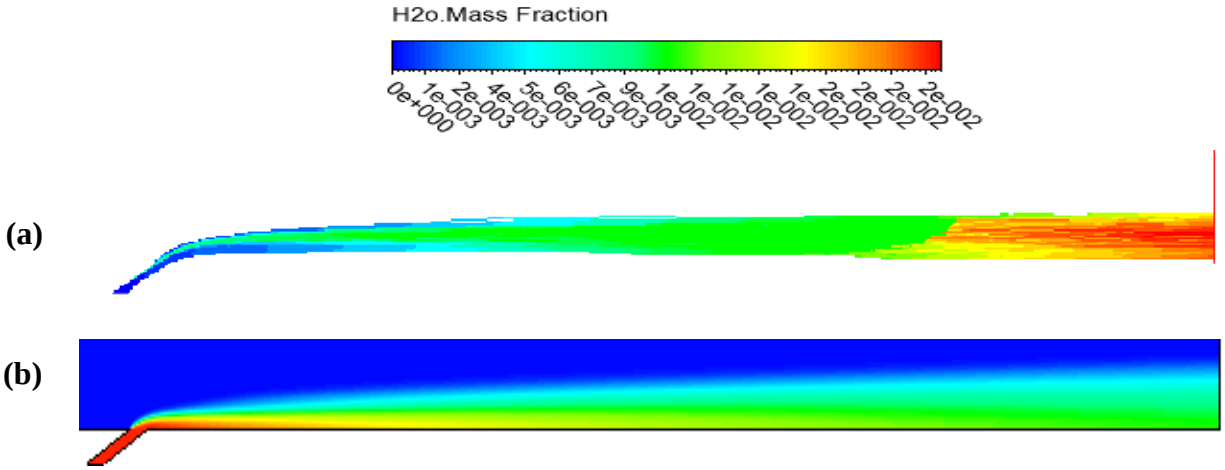

Figure 12. For Case1 at 10µm droplets, DR=2.74, BR=1.097, and Re_m = 61760 (a) Droplet trajectories predicted with stochastic tracking (b) Variation of H_2O mass Figure in the mainstream flow.

Particles track demonstration and variation of H2O mass fraction:

Droplet trajectories are predicted by employing stochastic tracking model. The stochastic tracking model incorporates the turbulent dispersion which tends to bring the particles closer to the wall surface to enhance the low temperature regions. Simulations were performed for DR=2.74, BR=1.097, and Re_m=61760 while considering the optimal diameter of droplets as 10µm for Case3

as depicted in Figure 12a. It is quite evident that when the water droplets encounter the mainstream flow, their temperature rises and they are heated up. Hence water droplets start evaporating in the mainstream flow yielding blanket effect of the cooling layer while protecting the blade surface from the mainstream flow. It is quite obvious that for both cases water droplets survive till the outlet at the far end of downstream region providing better cooling effectiveness. The crucial factors which impart noticeable role in this phenomenon are droplets diameter, mist injection rate, allocation and geometric configuration of deposition and fluid mechanical variables. In Figure 12b contour portrays the variation of H_2O mass fraction in the mainstream region. It can be perceived that the mass fraction of water is maximum in the coolant channel and it tends to decreasing due to evaporation in the mainstream flow providing significant increment in film cooling effectiveness.

Conclusions

Exploration of various cooling techniques of GT hot sections components motivated the authors to further pursue the quest for improvement of conventional cooling techniques and avail substantial enhancement in cooling effectiveness. This paper investigates the impact of small amount of mist injection (2%-mist rate) into coolant jet and airfoil as deposition on film cooling effectiveness. The vast range of fluid mechanical variables (ratios of density, velocity, mass flux and momentum flux) and their impact on local and average centerline film cooling effectiveness is investigated. The decisive conclusions of this numerical and parametric study are presented in the following.

- The presence of deposition increases the lower temperature regions and covers a large cooling area in downstream region hence higher local (η) and average centerline film cooling effectiveness ($\overline{\boldsymbol{\eta}}$) is achieved e.g. at X/D=30 for BR=2.05, DR=2.74 and $\Re_m$=61760 in the presence of airfoil deposition η is 8.33% higher than without deposition while, at same fluid mechanical variable $\overline{\boldsymbol{\eta}}$ in the presence of deposition is 5.64% higher than baseline case.
- The small amount of mist injection (2%) in coolant jet impart noteworthy role in obtaining desired local and average cooling effectiveness e.g. with the mist injection at X/D=35 for BR=3.01, DR=2.74 and $\Re_m$=61760 without deposition η is 16.45% higher than without mist injection model while at the same ratios and mainstream Reynold number 10.58% average centerline cooling effectiveness ($\acute{\eta}$ is obtained.
- The combination of both airfoil deposition and injection of water droplets in coolant jet provide even higher cooling effectiveness as the coolant jet prevails in far downstream region exposed to hot mainstream flow e.g. for BR=3.01, DR=2.74 and $\Re_m$=61760 at X/D=50 the local centerline cooling effectiveness is 23.6% higher than baseline case while at the same fluid mechanical variables 13.24% average centerline cooling effectiveness ($\overline{\boldsymbol{\eta}}$) is achieved.
- The enhancement in ratios of mass flux, velocity, momentum and density impart noteworthy impact on fluid flow behavior of coolant jet and mainstream which in results yield augmented cooling effectiveness. However, the excessive increment in blowing ratio tends to degrade the cooling performance e.g. for Case1 at BR=3.01 and DR=2.74, $\overline{\boldsymbol{\eta}}$ is 2.6% higher than at BR=5.0 and DR=2.74. Therefore, the optimum values for BR and DR found in this study are 3.01 and 2.74 respectively.

References

[1] J.-C. Han, S. Dutta, and S. Ekkad, Gas turbine heat transfer and cooling technology. 2012: CRC press.

[2] A. Sinha, D. Bogard and M. Crawford, Film-cooling effectiveness downstream of a single row of holes with variable density ratio. Journal of Turbomachinery, vol 113(3), pp. 442-449, 1991.

[3] J. B. Anderson, et al., Effects of Freestream Mach Number, Reynolds Number, and Boundary Layer Thickness on Film Cooling Effectiveness of Shaped Holes. in ASME Turbo Expo 2016: Turbomachinery Technical Conference and Exposition. American Society of Mechanical Engineers, 2016.

[4] J.-s. Wei, et al. Experimental study on the film cooling characteristics of the cylindrical holes embedded in sine-wave shaped trench. in ASME Turbo Expo 2016: Turbomachinery Technical Conference and Exposition. American Society of Mechanical Engineers, 2016.

[5] K. Singh, B. Premachandran and M. Ravi, A numerical study on the 2d film cooling of a flat surface. Numerical Heat Transfer, Part A: Applications, vol 67(6), pp. 673-695, 2015.

[6] K. Singh, et al., Prediction of film cooling effectiveness over a flat plate from film heating studies. Numerical Heat Transfer, Part A: Applications, vol 69(5), pp. 529-544, 2016.

[7] R. Jia, et al., A numerical and experimental investigation of the slot film-cooling jet with various angles. Journal of Turbomachinery, vol 127(3), pp. 635-645, 2005.

[8] K. Singh, B. Premachandran and M. Ravi, Experimental and numerical studies on film cooling with reverse/backward coolant injection. International Journal of Thermal Sciences, vol 111, pp. 390-408, 2017.

[9] M. Al-Hemyari, M. O. Hamdan and M. F. Orhan, A numerical analysis of the slot film-cooling effectiveness. in 2018 Advances in Science and Engineering Technology International Conferences (ASET), IEEE, 2018.

[10] M. Al-Hemyari, M .O. Hamdan and M. F. Orhan, Numerical analysis of film cooling effectiveness under variable blowing ratio and injection angles, Proceedings of the 3 rd World Congress on Momentum, Heat and Mass Transfer (MHMT'18), 2018.

[11] R. S. Bunker, A review of shaped hole turbine film-cooling technology. Journal of heat transfer, vol 127(4), pp. 441-453, 2005.

[12] T. L .Bergman, et al., Fundamentals of heat and mass transfer, John Wiley & Sons, 2011.

[13] X. Li, and T. Wang, Two-phase flow simulation of mist film cooling on turbine blades with conjugate internal cooling. Journal of Heat Transfer, vol 130(10), pp. 102901, 2008.

[14] X. Li, and T. Wang, Simulation of cooling enhancement with mist injection, Journal of Heat transfer, vol 128(6), pp. 509-519, 2006